Structural Engineering and Mechanics, *Vol. 69, No. 2 (2019) 221-230*
DOI: https://doi.org/10.12989/sem.2019.69.2.221

Shear behavior of non-persistent joints in concrete and gypsum specimens using combined experimental and numerical approaches

Hadi Haeri[1], V. Sarfarazi[2], Zheming Zhu*[1], N. Nohekhan Hokmabadi[3], MR. Moshrefifar[3] and A. Hedayat[4]

[1]*MOE Key Laboratory of Deep Underground Science and Engineering, School of Architecture and Environment, Sichuan University, Chengdu 610065, China*
[2]*Department of Mining Engineering, Hamedan University of Technology, Hamedan Iran*
[3]*Geology Department, Yazd University, Yazd, Iran*
[4]*Department of Civil and Environmental Engineering, Colorado School of Mines, Golden, CO 8040, USA*

(Received June 18, 2018, Revised December 12, 2018, Accepted December 15, 2018)

Abstract. In this paper, shear behavior of non-persistent joint surrounded in concrete and gypsum layers has been investigated using experimental test and numerical simulation. Two types of mixture were prepared for this study. The first type consists of water and gypsum that were mixed with a ratio of water/gypsum of 0.6. The second type of mixture, water, sand and cement were mixed with a ratio of 27%, 33% and 40% by weight. Shear behavior of a non-persistent joint embedded in these specimens is studied. Physical models consisting of two edge concrete layers with dimensions of 160 mm by 130 mm by 60 mm and one internal gypsum layer with the dimension of 16 mm by 13 mm by 6 mm were made. Two horizontal edge joints were embedded in concrete beams and one angled joint was created in gypsum layer. Several analyses with joints with angles of 0°, 30°, and 60° degree were conducted. The central fault places in 3 different positions. Along the edge joints, 1.5 cm vertically far from the edge joint face and 3 cm vertically far from the edge joint face. All samples were tested in compression using a universal loading machine and the shear load was induced because of the specimen geometry. Concurrent with the experiments, the extended finite element method (XFEM) was employed to analyze the fracture processes occurring in a non-persistent joint embedded in concrete and gypsum layers using Abaqus, a finite element software platform. The failure pattern of non-persistent cracks (faults) was found to be affected mostly by the central crack and its configuration and the shear strength was found to be related to the failure pattern. Comparison between experimental and corresponding numerical results showed a great agreement. XFEM was found as a capable tool for investigating the fracturing mechanism of rock specimens with non-persistent joint.

Keywords: non-persistent joints; uniaxial test; shear behaviour; experimental and numerical approaches

1. Introduction

Understanding rock mass behavior is of great importance because of its role in stability of rock structures (slopes, foundations, and tunnels) as well as fracturing processes such as blasting and hydraulic fracturing. Also, understanding brittle rock fracturing and failure is a prerequisite for understanding the rock mass behavior because rock fracturing has applications in underground structures, rock slopes and dam abutments, rock bursts in mining, wellbore stability, hydraulic fracturing, and geothermal reservoirs. The fracturing process in both intact rocks and rocks with pre-existing flaws (fractures) involves the initiation of new cracks their propagation, and coalescence (linkage) with pre-existing fractures.

Laboratory studies of fracture initiation, propagation, and coalescence have been extensively used and proved to be instrumental in understanding fracturing processes in brittle materials. Crack coalescence in rock-like and natural materials and concrete specimens (e.g., Whittaker and Singh 1992, Shen 1995, Bobet and Einstein 1998, Belytschko and Black 1999, Silling 2000, Wong and Einstein 2008, Peng 2009, Grenon and Hadjigeorgiou 2008, Singh *et al.* 2008, Park and Bobet 2009, Gischig *et al.* 2011, Feng *et al.* 2011, Zare Naghadehi *et al.* 2011, Zhou *et al*. 2012, Regmi *et al.* 2013, Sharma *et al.* 2013, Ramadoss 2013, Pan 2014, Panaghi *et al.* 2015, Zhao 2015, Li *et al.* 2015, Shakti *et al.* 2015, Kequan 2015, Wei *et al.* 2015, Zhou *et al*. 2015, Zhou *et al*. 2015, Li *et al.* 2016, Li *et al.* 2016, Haeri and Sarfarazi 2016, Yaylac 2016, Wang *et al.* 2017, Shemirani *et al.* 2017, Nabil *et al.* 2017, Monfared 2017, Bi *et al*. 2016, Bi *et al*. 2017, Yunteng *et al*. 2017, Boumaaza *et al.* 2017, Haeri *et al.* 2017, 2018, Lee and Lee 2018, Wang 2016, 2017, 2018, Wang *et al*. 2018, Rezaiee-Pajand and Gharaei-Moghaddam 2018) were extensively studied, and a nearly complete picture of fracturing, and the coalescence patterns for isotropic materials with dominantly open flaws currently exists. Both natural rocks and rock-like materials show similar fracturing patterns and the two common types of cracks commonly observed in specimens with pre-existing flaws subjected to uniaxial compression include wing cracks and secondary cracks. Wing cracks initiate at the tip of pre-existing flaws and propagate in a stable manner and in a curvilinear path and then align with the direction of the maximum compressive load (Bobet and Einstein 1998). Secondary cracks initiate later than the wing

*Corresponding author, Professor
E-mail: zhemingzhu@hotmail.com

http://www.techno-press.com/journals/sem&subpage=7
ISSN: 1225-4568 (Print), 1598-6217 (Online)

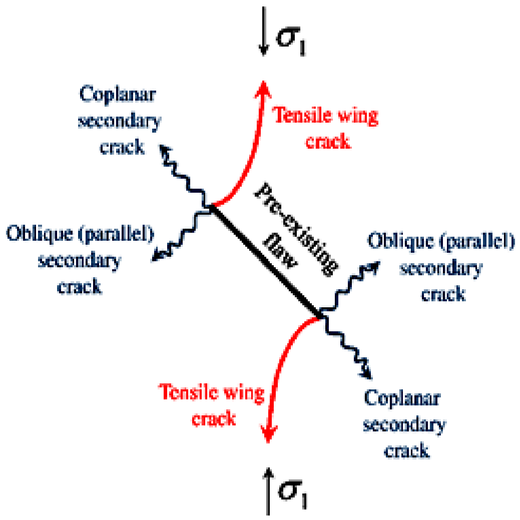

Fig. 1 Crack pattern in specimens with a pre-existing flaw in uniaxial compression (after Bobet and Einstein 1998)

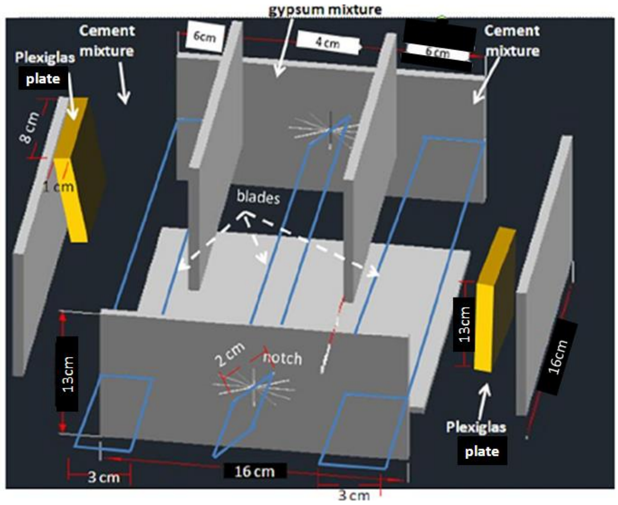

Fig. 2 The special mold consisting blades, mixture plates and Plexiglas plate

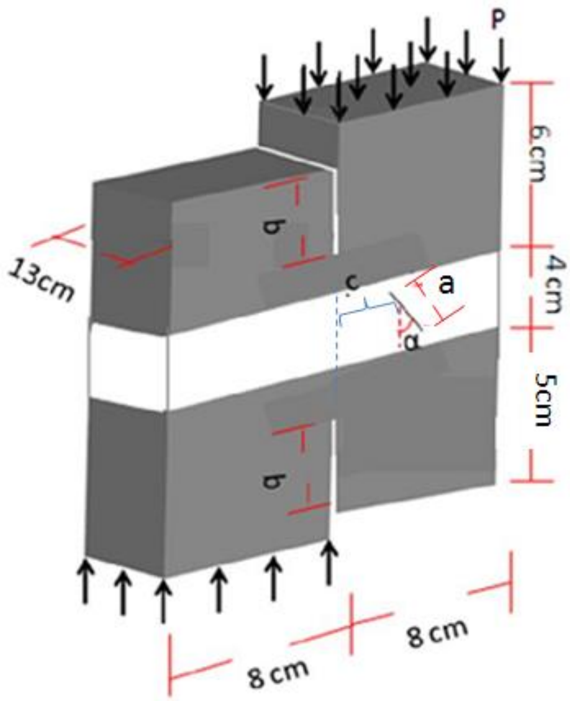

Fig. 3 Model geometry

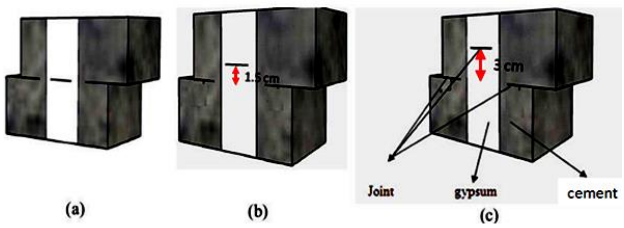

Fig. 4 Central joint is placed (a) along the vertical edge joints, (b) at the distance of 1.5 cm from the central joints, and (c) at a distance of 3 cm from the central joints

cracks and are considered as shear cracks that initiate mostly in the direction co-planar to the flaw. In specimens with multiple pre-existing flaws, a combination of wing and secondary cracks occur and result in the specimen failure. Fig. 1 shows the crack patterns commonly observed in specimens of rock materials with a single oriented flaw subjected to uniaxial compression.

The two initiation directions of the secondary crack, coplanar and oblique, were not observed in all the past studies. Many of studies only observed coplanar secondary cracks (Bobet and Einstein 1998), which is an indication that the direction of secondary cracks is material-dependent. Although most of the experimental studies considered secondary cracks as shear cracks, some studies showed that the secondary cracks that occur after the initiation of tensile wing cracks are not necessarily shear cracks and can be tensile in nature (Huang *et al.* 1990, Wong and Einstein 2009). The surface of shear cracks typically includes crushed and pulverized material with a rough texture (Park and Bobet 2010) while the surface of tensile cracks lacks any pulverized material.

Crack coalescence, as the linkage of flaws, occurs due to the initiation, propagation, and interaction of pre-existing and new cracks. The cracks observed in different coalescence patterns can typically be categorized into three groups: (a) tensile cracks, (b) mixed tensile-shear cracks, and (c) shear cracks. Several researchers have used a combination of experimental and numerical methods for evaluating the effect of distance between two co-planar cracks (e.g., Ghazvinian *et al.* 2012, Haeri 2015a, b, Sarfarazi and Haeri 2016a, b). Crack coalescence, as the linkage of flaws, occurs due to the initiation, propagation, and interaction of pre-existing and new flaws. Crack coalescence in rock-like materials (e.g., Shen 1995, Shen *et al.* 1995, Bobet and Einstein 1998, Sagong and Bobet 2002, Wong and Einstein 2007, 2009) and natural materials (e.g., Lee and Jeon 2011) were extensively studied, and a nearly complete picture of fracturing, and the coalescence patterns for isotropic materials with dominantly open flaws currently exists. Although significant progress has been made in characterizing the failure mechanism of isotropic materials and in single layer, there is still a need for characterizing the failure pattern and failure mechanism of non-persistent cracks (faults) situated in two different layers. This study focuses on the failure mechanism of non-persistent cracks using a combined experimental and numerical approach.

2. Specimen preparation and testing

2.1 Specimen preparation

Two types of mixture were prepared for this study. The first type consists of water and gypsum that were mixed with a ratio of water/gypsum of 0.6. The second type of mixture, water, sand and cement were mixed with a ratio of 27%, 33% and 40% by weight. The materials were mixed carefully, casted in molds, and cured following the same procedure to obtain homogeneous, isotropic, and repeatable samples. The pastes were poured into special mold (Fig. 2). This mold consists of three different boxes with the dimensions shown in Fig. 2. Two Plexiglas plates with dimensions of 80 mm by 130 mm by 10 mm were made and put at the mold's top and bottom surfaces to create the special geometry of the block. Immediately after casting the materials, the mold was vibrated to remove any air entrapped air bubbles from the specimen. To create pre-existing joints in the specimens, metal blades with dimensions of 1 mm in thickness, 160 mm in length and widths of 20 and 30 mm, were used. Two blades with width of 30 mm were placed in the lateral boxes and blade with width of 20 mm was placed in the central box (Fig. 2). For the condition shown in Fig. 2, the length of the marginal faults (b) is 30 mm and the length of the central fault (a) is 20 mm with opening of 1 mm (Fig. 3). The central shim was placed in one of the following configurations: (1) along the edge joints, (2) 15 mm eccentric from the symmetrical line, and (3) 30 mm eccentric from symmetrical line (Fig. 4). The angle of central joint (α) varied between 0°, 30°, and 60° (Fig. 3). After 24 hours of curing at room temperature and in the mold, the specimen was unmolded and cured at room condition with the temperature of 20°±2°C for 14 days. A total of 9 specimens were made and successfully tested for investigation of shear behavior of non-persistent joints.

2.2 Specimen testing

The tests were performed using a 2000 KN loading machine. The testing was conducted with a constant rate of deformation of 0.01 mm/s between the rigid loading platens of the machine. In this configuration, the applied normal load induces shear stresses along the embedded central joints and in the intact gypsum layer (Figs. 3-4). A data acquisition system was used for recording the applied normal load as well as the vertical displacement (compression) applied at the two ends of the specimen.

3. Experimental results

For different scenarios, the observed fracturing pattern is presented and discussed in this section. Fig. 5 shows the different failure modes in specimen with the central joint. The inspection of failure surfaces shows that the failure surfaces were smooth and without any crushed or pulverized materials. This is a good indication that the tensile failure mode occurred in all specimens and geometries.

3.1 Central joint placed along the two vertical edge joints with the angularity of 0°

The length of each rock bridge on the sides of central joint is 2.5 cm (Fig. 5(a)). The cracks initiated from the tip of the edge joints and propagated towards the central joint. By increasing the normal loading, the cracks reached the gypsum-cement boundaries and grew diagonally. These cracks then coalesced with the tips of the central joint. This coalescence left two oval cores of cement/gypsum materials.

3.2 Central joint placed at the distance of 1.5 cm from the alignment of the two edge joints with the angularity of 0°

In this configuration (Fig. 5(b)), cracks initiated form the tip of the left edge joint and propagated with direction of 45° degree with respect to the loading direction. This crack reached the gypsum-cement boundary and then propagated horizontally till coalesced with the tip of the central joint. The other crack initiated from the edge of the specimen and propagated towards the gypsum-cement boundary. This crack grew horizontally in the gypsum layer and then coalesced with the central joint. This coalescence left an echelon failure in the sample (Fig. 5(b)).

3.3 Central joint placed at the distance of 3 cm from the alignment of the two edge joints with the angularity of 0°

The rock bridge on both sides of the central fault is 3 cm. In this configuration, crack initiated from tip of the left edge joint and propagate horizontally till coalesce with right side of the cement-gypsum boundary. This crack propagates with direction of 30° degree related to horizontal line and coalesces with left side of cement-gypsum boundary. Other crack initiates from tip of the right edge joint and propagates toward the right side of the gypsum-cement boundary with direction of -10° degree related to horizontal line. This crack grows in gypsum with direction of 10° degree related to horizontal line and coalescence with another crack tip. This coalescence left a wavy failure surface in the sample (Fig. 5(c)).

3.4 Central joint placed along the two vertical edge joints with the angularity of 30°

In this configuration (Fig. 5(d)), the length of rock bridges at each side is 3 cm. First crack initiated form tip of the right edge joint and propagated horizontally along the joint plane. This crack reached the gypsum-cement boundary and then propagated horizontally and reached the central joint. The other crack initiated from the left side of the specimen and propagated towards the gypsum-cement boundary. With an additional propagation in the gypsum material, this crack reached the tip of the central crack. This second cracking event left a wavy failure surface in the specimen (Fig. 5(d)).

3.5 Central joint placed at the distance of 1.5 cm from the alignment of the two edge joints with the angularity of 30°

In this configuration as shown in Fig. 5(e), the cracking stared from the tip of the right edge joint, as shown with the number 1 in the Figure, and propagated with direction of 45° degrees with respect to the horizontal line. This crack reached the gypsum-cement boundary and then propagated towards the tip of the central crack. The other cracking started at the left joint wall and propagated parallel to the shear load direction and reached the gypsum-cement boundary. After arresting at the boundary and propagating along the boundary, a new crack was formed and propagated horizontally in gypsum material until it coalesced with the tip of the central joint (Fig. 5(e)).

3.6 Central joint placed at the distance of 3 cm from the alignment of the two edge joints with the angularity of 30°

In this configuration (Fig. 5(f)), cracking started from the tip of the right edge joint and propagated with direction of 45° degree related to horizontal direction. This crack reached the gypsum-cement boundary and then propagated with the direction of 45 degree with the horizontal line and coalesced with the right side of the central joint. On the left side of the specimen (Fig. 5(f)), a new crack initiated from the edge joint and propagated parallel to shear load direction till it reached the gypsum-cement boundary. This crack was arrested at the boundary and was shifted along the boundary and then propagated inside the gypsum layer until it coalesced with the wall of the central joint (not the tip). This failure pattern was wavy and no coalescence with the left side tip of the central crack was observed.

3.7 Central joint placed along the two vertical edge joints with the angularity of 60°

In this configuration (Fig. 5(g)), cracks initiated form tips of the edge joints and propagated in the 45° degree direction with respect to the loading direction (i.e., horizontal line in this figure). These cracks reached the gypsum-cement boundaries and the coalesced with the tips of the central joint. As can be seen, this failure pattern is a great example of wing (tensile) crack propagation as shown in Fig. 1.

3.8 Central joint placed at the distance of 1.5 cm from the alignment of the two edge joints with the angularity of 60°

In this configuration (Fig. 5(h)), the first crack initiated from the tip of the right edge joint and turned downward after a small propagation distance. This crack propagated with a 15° degree orientation with the horizontal line and

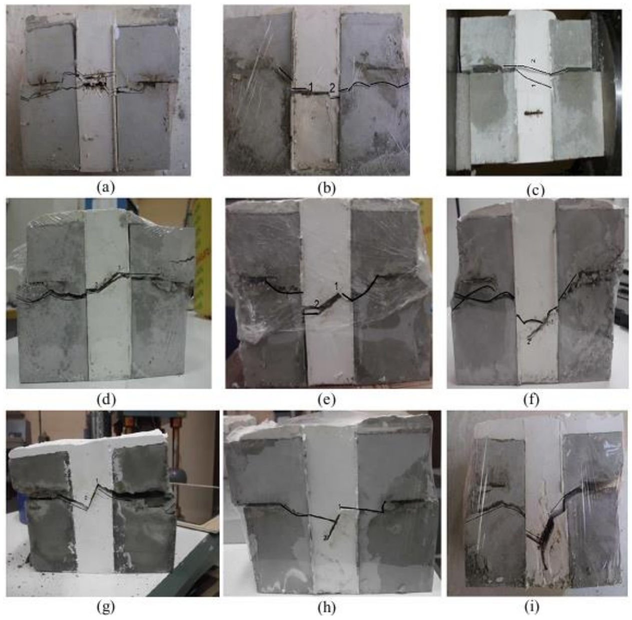

Fig. 5 Failure mode in specimen when the central joint placed (a) along the two vertical edge joints with the angularity of 0°, (b) 1.5 cm from the alignment of the two edge joints with the angularity of 0°, (c) 3 cm from the alignment of the two edge joints with the angularity of 0°, (d) along the two vertical edge joints with the angularity of 30°, (e) 1.5 cm from the alignment of the two edge joints with the angularity of 30°, (f) 3 cm from the alignment of the two edge joints with the angularity of 30°, (g) along the two vertical edge joints with the angularity of 60°, (h) 1.5 cm from the alignment of the two edge joints with the angularity of 60°, and (i) 3 cm from the alignment of the two edge joints with the angularity of 60°

reached the gypsum-cement boundary. This crack crossed the boundary and reached the central joint. The second major crack started at the left edge joint and reached the gypsum-cement boundary and finally reached the wall of the central fault. This coalescence left a stepped failure surface in the sample (Fig. 5(h)).

3.9 Central joint placed at the distance of 3 cm from the alignment of the two edge joints with the angularity of 60°

In this configuration (Fig. 5(i)), a crack initiated from the tip of the right edge joint and reached the gypsum-cement boundary. After propagation along the boundary, a new crack was formed and propagated towards the tip of the central joint. Similarly, a crack occurred from the left edge of the specimen and developed in nearly a parallel direction to the shear load until it reached the gypsum-cement boundary. After shifting along the boundary, the crack propagated diagonally in gypsum material and reached the tip of the central joint.

It's to be noted that shear cracks, such as coplanar secondary cracks and oblique secondary cracks were created in oriented joints.

4. Numerical simulations

The extended finite element method (XFEM) has proved to be a very successful technique in simulating the fracture processes in brittle materials including both concrete and geomaterials (Mariani And Perego 2003, Feng *et al.* 2011, Hedayat *et al.* 2015). The XFEM method allows for the analysis of crack initiation and propagation along an arbitrary path without the need for remeshing. This paper uses XFEM through the finite element software platform-Abaqus version 6.11 to predict the crack propagation in concrete/gypsum layer that consists a non-persistent joint.

4.1 Theory of extended finite element method

The extension of the finite element formulation to provide an approximate solution for discontinuities in the solution domain by enriching the domain with additional nodes is referred to Extended Finite Element (XFEM). In this formulation the discontinuities or the flaws are represented independently from the continuous domain. As such, the need for re-meshing to capture the evolution of new discontinuous features (new surface), such as crack propagation and branching, is eliminated. The initial mesh will have nodes at the tip of the existing closed flaw. At each loading increment, the fracture process zone (FPZ) is enriched with nodes that allows for crack propagation. The discontinuous displacement field is then represented by an enrichment function that captures the discontinuity in the displacement field, allowing for crack changing aperture.

To introduce the enrichment functions assume a nodal set {I} and a subset of the nodes to be enriched {I1}, such that {I1} ⊂ {I} then the displacement at nodal level could be given as the classical finite element plus the enrichment function (Fries *et al.* 2000)

$$u^h(x) = \sum_{i \in I} N_i(x) u_i + \sum_{i \in I^1} N_i^1(x) \psi_i(x) a_i \tag{1}$$

Such that

$$\sum_{i \in I^1} N_i^1(x) \psi_i(x) = \psi_i(x) \tag{2}$$

where $u^h(x)$ is approximated function, $N_i(x)$ is the FE standard shape function, u_i is FE degrees of freedom, a_i is the extra degrees of freedom, $\psi_i(x)$ is the global enrichment function, N_i^1 is the partition of unity function, and $\sum_{i \in I^1} N_i^1(x)$ is equal to 1.

The global enrichment function is usually selected as a Heaviside function with a value of 1 on one side of the crack and -1 on the other side of the crack. Generally, for jump and enrichment functions along the side of the crack and near the crack tip, Eq. (1) is given as

$$\begin{aligned} u^h(x) &= \sum_{i \in I} N_i(x) u_i + \sum_{i \in I^1} N_i^1(x) \psi_i^1(x) a_i^1 \\ &+ \sum_{i \in I^2} N_i^2(x) \psi_i^2(x) a_i^2 \end{aligned} \tag{3}$$

where I^1 and I^2 are the nodal subset at the crack tip and along the crack length, respectively, $\psi_i^1(x)$ and $\psi_i^2(x)$ are tip enrichment and jump functions. The tip enrichment and jump function appears in the element stiffness matrix as follows

$$[K_e] = \int_v [B]^T [D][B] dv \tag{4}$$

where,

$$[B] = [\partial][N(x)] \quad \text{for continuous domain,} \tag{5}$$

$$[B^1] = [\partial][N_i^1(x) \psi_i^1(x)] \quad \text{for tip enrichment,} \tag{6}$$

$$[B^2] = [\partial][N_i^2(x) \psi_i^2(x)] \quad \text{for jump function.} \tag{7}$$

The above equations are used in the weak form solution to develop the element stiffness matrix.

Table 1 Parameters of concrete using XFEM

Young Modulus (MPa)	Poisson's ratio	Density	MAXPS Damage (MPa)	GI(N/m)	GII(N/m)	GIII(N/m)
26800	0.19	2800	2.9	250	250	250

Table 2 Parameters of gypsum using XFEM

Young Modulus (MPa)	Poisson's ratio	Density	MAXPS Damage (MPa)	GI(N/m)	GII(N/m)	GIII(N/m)
10200	0.24	2200	1.5	110	110	110

4.2 Numerical simulation of concrete/gypsum specimen with a non-persistent joint

Failure of concrete-gypsum specimen with two edge cracks and one internal crack under applied loading conditions was simulated using XFEM in the FEM software platform Abaqus version 6.11 (Fig. 6). A box model consisting of two concrete beams and one internal gypsum beam was created in Abaqus to model the direct shear setup. Two edge joints were situated in concrete beam and one internal joint was situated in gypsum layer. The model region of two edge concrete beams is 60 mm×160 mm×130 mm with two edge cracks and the model region of surrounded gypsum beams is 40 mm×160 mm×130 mm with one internal crack (Fig. 6).

The position of edge cracks is fixed and their lengths were 3 cm. The position of internal cracks is variable and its length was 2 cm. The central crack was situated in three different situations (c) (Fig. 6), i.e., along the edge joints (c=0), 1.5 cm far from symmetrical line and 3 cm far from symmetrical line. The angle of central joint (α) varied from 0° to 60° with increment of 30° (Fig. 6). Material parameters for concrete and gypsum are shown as Table 1-2.

The movement of wall id 6, 7, 8, 9, and 10 was constrain in both of the x and y direction while wall id=1, 2, 3, 4, and 5 were moved freely in x direction (Fig. 7(a)). The loading was applied at the right side of the model by movement of wall id 1 at opposite side of x direction with a

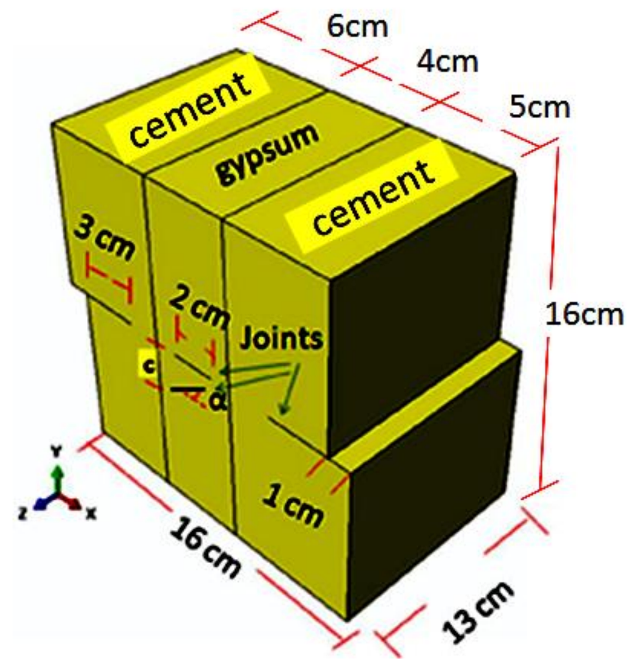

Fig. 6 The concrete/gypsum beam with initial and edge cracks

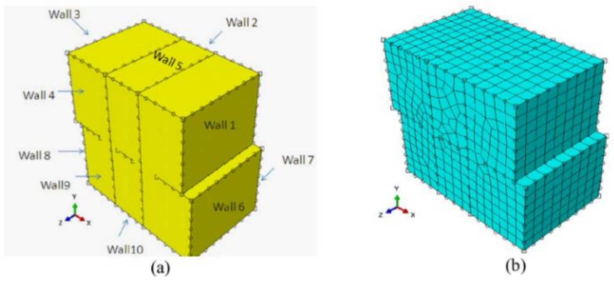

Fig 7(a) identification of model surfaces boundaries, (b) meshing with 8-node linear brick

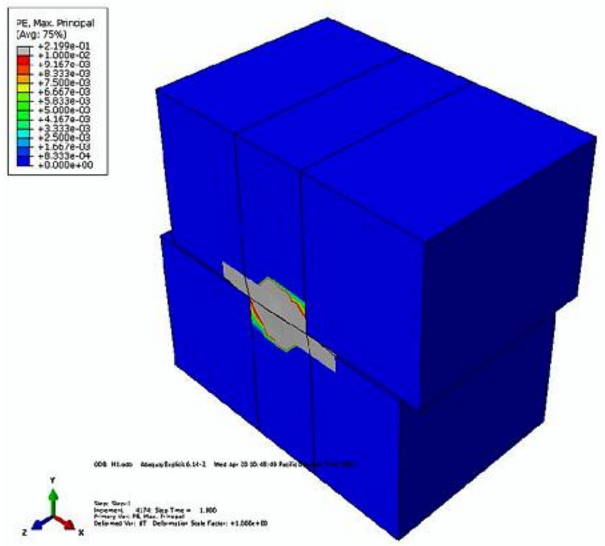

Fig. 8 final crack propagation with max principal stress contours when internal joint angularity is 0°

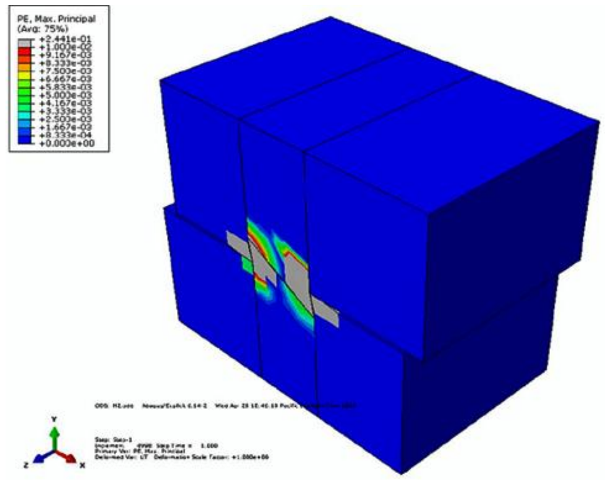

Fig. 9 final crack propagation with max principal stress contours when internal joint angularity is 30°

velocity of 0.016 mm/s. The loading will induce cracks that reach the concrete beam. The ultimate load can be determined from the reaction force curve. The FEM model with the boundaries and meshes are shown in Fig. 7. The surfaces between cement and gypsum in numerical simulation were set by interface element which has the high tensile strength.

4.3 Numerical results

In this section, effect of internal joint (flaw) position on the shear failure behavior of concrete/ gypsum beam has been analyzed.

a) Internal joint was situated in a distance of 0 from edge crack face

Figs. 8-10 show final crack propagation with max principal stress contours for different internal joint angularities. Internal joint was situated in a distance of 0 from edge crack face. Gray color and blue color show the region with high stress and low stress, respectively. Fig. 8 shows that when internal joint angularity is 0°, maximum principal stress was distributed in vicinity of internal joint and at tip of the edge joint. In this condition damage zone is like a fish eye and distributed in rock bridge area. By comparison between Fig. 8 and Fig. 5(a), it can be concluded that the same failure pattern was occurred in this model. When internal joint angularity was 30° (Fig. 9), maximum principal stress was distributed in vicinity of internal joint and at tip of the edge joint but its extent was larger than previous case. In this condition two damage zone like a fish eye were formed patricianly in upper and lower of the internal joint. Also, two small damage zones were formed near the edge joints. By comparison between Fig. 9 and Fig. 5(b), it can be concluded that the same failure pattern was occurred in this model.

When internal joint angularity was 60° (Fig. 10), maximum principal stress was distributed in vicinity of internal joint and at tip of the edge joint but its extent was larger than two previous cases. In this condition two triangle shape damage zone were formed completely in upper and lower of the internal joint. Also, two small damage zones were formed near the edge joints. By

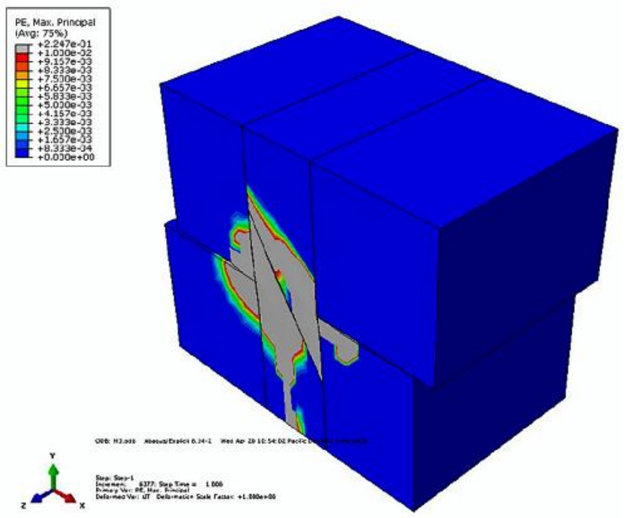

Fig. 10 final crack propagation with max principal stress contours when internal joint angularity is 60°

comparison between Fig. 10 and Fig. 5(c), it can be concluded that the same failure pattern was occurred in this model.

b) Internal joint was situated in a distance of a from edge crack face

Figs. 11-13 show final crack propagation with max principal stress contours for different internal joint angularities. Internal joint was situated in a distance of a from edge crack face. Gray color and blue color show the region with high stress and low stress, respectively. Fig. 11 shows that when internal joint angularity is 0°, maximum principal stress was distributed in vicinity of internal joint and at tip of the edge joint. Also, maximum principal stress was distributed vertically in middle of the model. In this condition damage zone is like a fish eye and distributed in rock bridge area. Two small damage zones were created at tip of the joint and two vertical damage band initiates from fish eye damage zone and coalesce to the model edge. It's to be note that internal joint has been participated in failure process. By comparison between Fig. 11 and Fig. 5(d), it can be concluded that the same failure pattern was occurred in this model. When internal joint angularity was 30° (Fig. 12), maximum principal stress was distributed between the edge joints. In this condition a big damage zone was formed in lower of the internal joint. Also, one small damage zones were formed near the left edge joint. By comparison between Fig. 12 and Fig. 5(e), it can be concluded that the same failure pattern was occurred in this model.

When internal joint angularity was 60° (Fig. 13), maximum principal stress was distributed in vicinity of internal joint and at tip of the edge joint but its extent was larger than two previous cases. In this condition two triangle shape damage zone were formed in upper and lower of the internal joint. Also, two small damage zones were formed near the edge joints. By comparison between Fig. 13 and Fig. 5(f), it can be concluded that the same failure pattern was occurred in this model.

c) Internal joint was situated in a distance of 2a from edge crack face

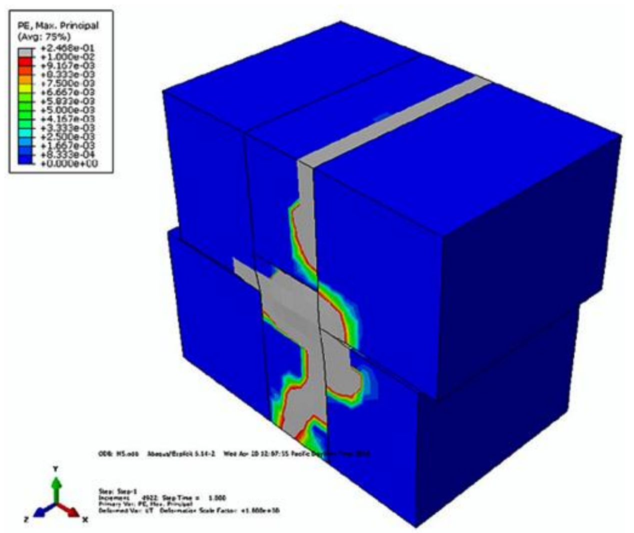

Fig. 11 final crack propagation with max principal stress contours when internal joint angularity is 0°

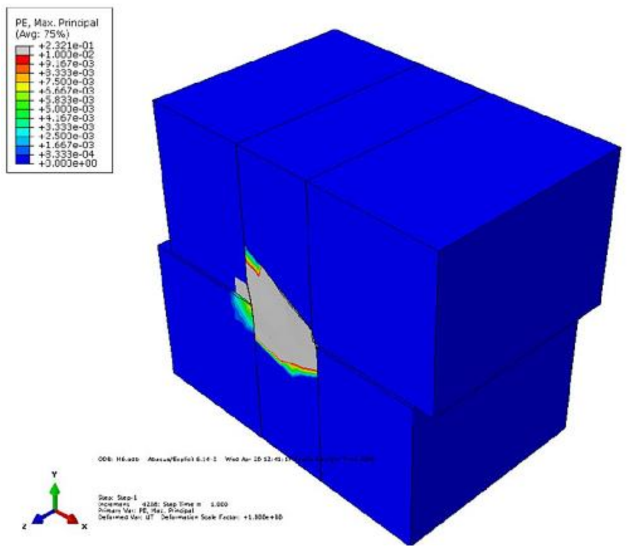

Fig. 12 final crack propagation with max principal stress contours when internal joint angularity is 30°

Figs. 14-16 show final crack propagation with max principal stress contours for different internal joint angularities. Internal join was situated in a distance of 2a from edge crack face. Gray color and blue color show the region with high stress and low stress, respectively. Fig. 14 shows that when internal joint angularity is 0°, maximum principal stress was distributed between the edges joint (Rock Bridge) and internal joint is far from the critical stress zone. In this condition, damage zone like a fish eye distributed in rock bridge area. Two small damage zones were created at tip of the joint. It's to be note that internal joint has not any effects on the rock bridge failure. By comparison between Fig. 14 and Fig. 5(g), it can be concluded that the same failure pattern was occurred in this model.

When internal joint angularity was 30° (Fig. 15), maximum principal stress was distributed between the edge joints. In this condition a big damage zone was formed in

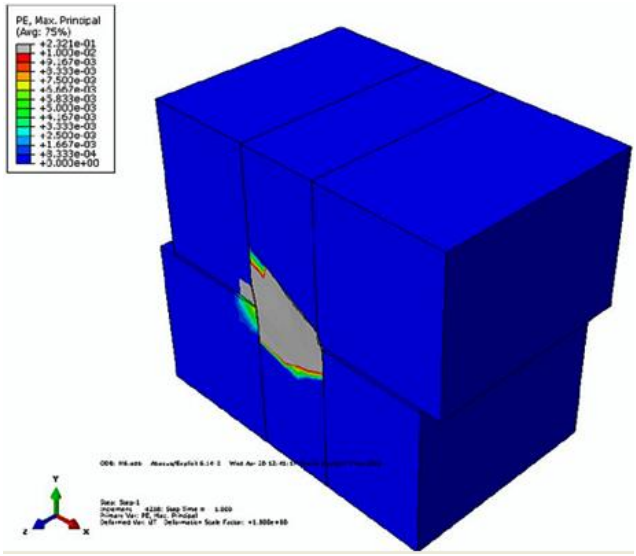

Fig. 13 final crack propagation with max principal stress contours when internal joint angularity is 60°

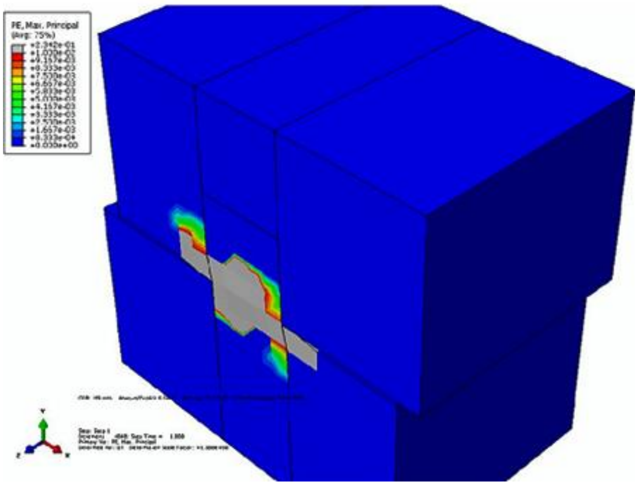

Fig. 14 final crack propagation with max principal stress contours when internal joint angularity is 0°

lower of the internal joint. Also, one small damage zones were formed near the left edge joint. By comparison between Fig. 15 and Fig. 5(h), it can be concluded that the same failure pattern was occurred in this model.

When internal joint angularity was 60° (Fig. 16), maximum principal stress was distributed between the edge joint and internal joint is out of critical stress distribution. In this condition two narrow damage zone were formed diagonally in upper and lower of the internal joint. Also, two small damage zones were formed near the edge joints. By comparison between Fig. 16 and Fig. 5(i), it can be concluded that the same failure pattern was occurred in this model.

d) Variation final stress with internal joint angle and internal joint spacing

Fig. 17(a) and (b) shows variation of final stress versus internal joint angle for experimental test and numerical results, respectively. Spacing of internal joint from edge joint was 0, 1.5 mm and 3 mm.

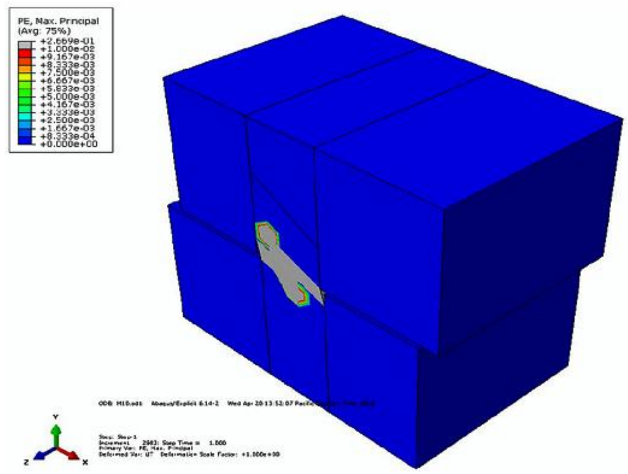

Fig. 15 final crack propagation with max principal stress contours when internal joint angularity is 30°

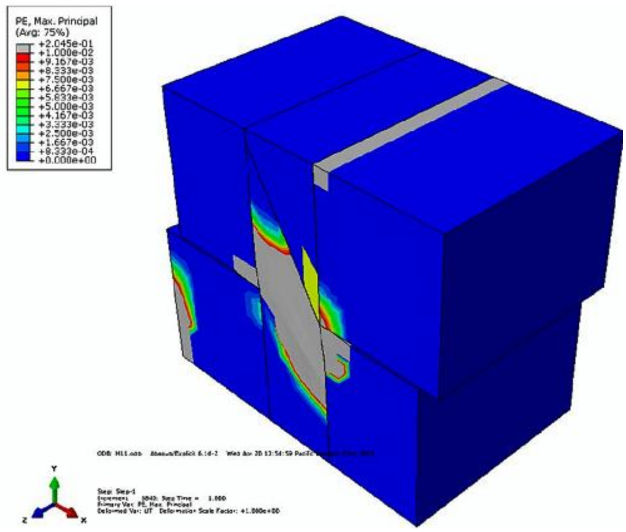

Fig. 16 final crack propagation with max principal stress contours when internal joint angularity is 60°

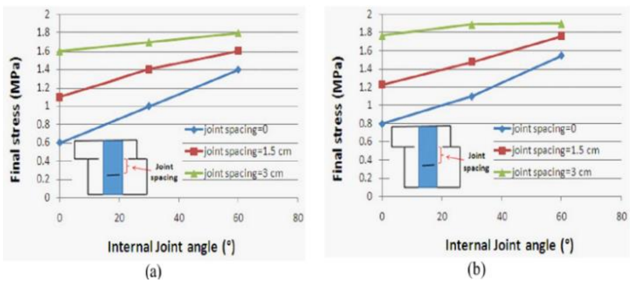

Fig. 17 Variation of final stress versus internal joint angle for (a) experimental test and (b) numerical results

Fig. 17 shows that final stress increases with increasing the joint angle. The increasing rate was high when joint spacing is 0 cm but its rate was decreased with increasing the joint spacing. Comparison between Fig. 17(a) and (b) shows that the same results were established between experimental test and numerical simulation. It can be concluded that XFEM is a capable method for investigation of shear behavior of non-persistent joint.

5. Conclusions

In this paper, shear behavior of non-persistent joint surrounded in concrete and gypsum layers has been investigated using experimental test and numerical simulation. Physical model consisting two edge concrete layers and one internal gypsum layer has been built. Two horizontal edge joints with exist in concrete beams and one angled joint was created in gypsum layer. Angularity of the internal joint varies from 0° to 60° with increasing the 30°. All samples tested by uniaxial test machine so that shear load was distributed in the specimens due to special geometry of specimen. Also, the ABAQUS commercial package was used for the XFEM simulations.

The major concluding points can be summarized as follows:

• Tensile crack was the dominant mode of failure.

• The failure surface was wavy. With increasing the central joint angularity, the waviness of failure surface also increased.

• With increasing the distance between the edge joints and central joint, only edge joint participated in the failure process.

• Final stress increased as the internal joint angle increased. The increasing rate was high when joint spacing was 0 cm but its rate decreased with increasing the joint spacing.

• Comparison between experimental and numerical results showed a great agreement. XFEM was found as a capable tool for investigating the fracture process of concrete/gypsum beams with non-persistent joint.

References

Belytschko, T. and Black, T. (1999) “Elastic crack growth in finite element with minimal remeshing”, *Int. J. Numer. Meth. Eng.*, **45**(5), 601-620.

Bi, J., Zhou, X.P. and Qian, Q.H. (2016) “The 3D numerical simulation for the propagation process of multiple pre-existing flaws in rock-like materials subjected to biaxial compressive loads”, *Rock Mech. Rock Eng.*, **49**(5), 1611-1627.

Bi, J., Zhou, X.P. and Xu, X.M. (2017) “Numerical simulation of failure process of rock-like materials subjected to impact loads”, *Int. J. Geomech.*, **17**(3), 04016073.

Bobet, A. and Einstein, H.H. (1998), “Fracture coalescence in rock-type materials under uniaxial and biaxial compression”, *Int. J. Rock Mech. Min. Sci.*, **35**(7), 863-888.

Boumaaza, M., Bezazi, A., Bouchelaghem, H., Benzennache, N., Amziane, S. and Scarpa, F. (2017), “Behavior of pre-cracked deep beams with composite materials repairs”, *Struct. Eng. Mech.*, **63**(4), 43-56.

Cao, P. (2014), “Crack propagation and coalescence of brittle rock-like specimens with pre-existing crack in compression”, *Eng. Geol.*, **187**, 113-121.

Feng, D., Tian, L. and Peng, C. (2011), “Study of longitudinal cracking during settlement of soil based on extended finite element method”, *Eng. Mech.*, **28**(5), 149-154.

Fries, T.P. and Belytschko, T. (2000), “The extended/generalized finite element methods: An overview of the method and its applications”, *Int. J. Numer. Met. Eng.*, **84**(3), 1-6.

Ghazvinian, A., Sarfarazi, V., Schubert, W. and Blumel, M. (2012), “A study of the failure mechanism of planar non-persistent open joints using PFC2D”, *Rock Mech. Rock Eng.*, **45**(5), 677-693.

Gischig, V., Amann, F., Moore, J.R., Loew, S., Eisenbeiss, H. and Stempfhuber, W. (2011), “Composite rock slope kinematics at the current randa instability, Switzerland, based on remote sensing and numerical modeling”, *Eng. Geol.*, **118**(1-2), 37-53.

Grenon, M. and Hadjigeorgiou, J. (2008), “A design methodology for rock slopes susceptible to wedge failure using fracture system modeling”, *Eng. Geol.*, **96**(1-2), 78-93.

Haeri, H. (2015a), “Propagation mechanism of neighboring cracks in rock-like cylindrical specimens under uniaxial compression”, *J. Min. Sci.*, **51**(3), 487-496.

Haeri, H. (2015b), “Crack analysis of pre-cracked brittle specimens under biaxial compression”, *J. Min. Sci.*, **51**(6), 1091-1100.

Haeri, H. and Sarfarazi, V. (2016) “Experimental study of shear behavior of planar non-persistent joint”, *Comput. Concrete*, **17**(5), 639-653.

Haeri, H., Sarfarazi, V., Shemirani, A.B. and Hedayat, A. (2017), “Experimental and numerical investigation of the center-cracked horseshoe disk method for determining the mode I fracture toughness of rock-like material”, *Rock Mech. Rock Eng.*

Haeri, H., Sarfarazi, V., Shemirani, A.B. and Hedayat, A. (2018), “Determination of tensile strength of concrete using a novel apparatus”, *Constr. Build. Mater.*, **166**, 817-832.

Hedayat, A., Ochoa, F. and Khasawneh, Y. (2015), “Numerical simulation of crack initiation and growth in rock specimens containing a flaw under uniaxial compression”, *Proceedings of the 49th US Rock Mechanics Symposium*, San Francisco, June-Juuly.

Kequan, Y.U. and Zhoudao, L.U. (2015), “Influence of softening curves on the residual fracture toughness of post-fire normal-strength concrete”, *Comput. Concrete*, **15**(2), 102-111.

Lee, J.W. and Lee, J.Y. (2018), “A transfer matrix method for in-plane bending vibrations of tapered beams with axial force and multiple edge cracks”, *Struct. Eng. Mech.*, **66**(1), 45-68.

Li, J.Y., Zhou, H., Zhu, W. and Li, S. (2016), “Experimental and numerical investigations on the shear behavior of a jointed rock mass”, *Geosci. J.*, **20**(3), 371-379.

Li, S., Wang, H., Li, Y., Li, Q., Zhang, B. and Zhu, H. (2016), “A new mini-grating absolute di placement measuring system for static and dynamic geomechanical model tests”, *Measure.*, **82**, 421-431.

Li, Y., Zhou, H., Zhu, W., Li, S. and Liu, J. (2015), “Numerical study on crack propagation in brittle jointed rock mass influenced by fracture water pressure”, *Mater.*, **8**(6), 3364-3376.

Li, Y.P., Chen, L.Z. and Wang, Y.H. (2005), “Experimental research on pre-cracked marble”, *Int. J. Sol. Struct.*, **42**(9-10), 2505-2016.

Mariani, S. and Perego, U. (2003) “Extended finite element method for quasi-brittle fracture”, *Int. J. Numer. Meth. Eng.*, **58**(1), 103-126.

Monfared, M.M. (2017), “Mode III SIFs for interface cracks in an FGM coating-substrate system”, *Struct. Eng. Mech.*, **64**(1), 78-95.

Nabil, B., Abdelkader, B., Miloud, A. and Noureddine, B. (2012), “On the mixed-mode crack propagation in FGMs plates: Comparison of different criteria”, *Struct. Eng. Mech.*, **61**(3), 201-213.

Pan, B., Gao, Y. and Zhong, Y. (2014), “Theoretical analysis of overlay resisting crack propagation in old cement concrete pavement”, *Struct. Eng. Mech.*, **52**(4), 167-181.

Panaghi, K., Golshani, A. and Takemura, T. (2015), “Rock failure assessment based on crack density and anisotropy index variations during triaxial loading tests”, *Geomech. Eng.*, **9**(6), 793-813.

Park, C.H. and Bobet, A. (2010), “Crack coalescence in specimens with open and closed flaws”, *Int. J. Rock Mech. Min. Sci.*,

46(5), 819-829.
Park, C.H. and Bobet, A. (2009), "Crack coalescence in specimens with open and closed flaws: A comparison", *Int. J. Rock Mech. Min. Sci.*, **46**(5), 819-829.
Peng, C. (2009), "Plastic damage model of concrete and development of Abaqus UMAT", M.Sc. Dissertation, Shenyang University of Technology.
Ramadoss, P. and Nagamani, K. (2013), "Stress-strain behavior and toughness of high-performance steel fiber reinforced concrete in compression", *Comput. Concrete*, **11**(2), 55-65.
Regmi, A.D., Yoshida, K., Nagata, H., Pradhan, A.M.S., Pradhan, B. and Pourghasemi, H.R. (2013), "The relationship between geology and rock weathering on the rock instability along Mugling-Narayanghat road corridor, Central Nepal Himalaya", *Nat. Hazards*, **66**(2), 501-532.
Rezaiee-Pajand M. and Gharaei-Moghaddam N. (2018), "Two new triangular finite elements containing stable open cracks", *Struct. Eng. Mech.*, **65**(1), 46-71.
Sarfarazi, V. and Haeri, H. (2016a), "The effect of non-persistent joints on sliding direction of rock slopes", *Comput. Concrete*, **17**(6), 723-737.
Sarfarazi, V. and Haeri, H. (2016b), "Effect of number and configuration of bridges on shear properties of sliding surface", *J. Min. Sci.*, **52**(2), 245-257.
Shakti, S.P., Parhi, D.R. and Mishra, D. (2015), "Comparative study on cracked beam with different types of cracks carrying moving mass", *Struct. Eng. Mech.*, **56**(5), 33-45.
Sharma, R.K., Mehta, B.S. and Jamwal, C.S. (2013), "Cut slope stability evaluation of NH 21 along Nalayan-Gambhrola section, Bilaspur district, Himachal Pradesh, India", *Nat. Hazards*, **66**(2), 249-270.
Shemirani, A., Haeri, H., Sarfarazi, V. and Hedayat, A. (2017), "A review paper about experimental investigations on failure behavior of non-persistent joint", *Geomech. Eng.*, **13**(4), 535-570.
Silling, S.A. (2000), "Reformulation of elasticity theory for discontinuities and long-range forces", *J. Mech. Phys. Sol.*, **48**(1), 175-209.
Singh, T.N., Gulati, A., Dontha, L. and Bhardwaj, V. (2008), "Evaluating cut slope failure by numerical analysis-a case study", *Nat. Hazards*, **47**(2), 263-279.
Wang, Y., Zhou, X.P. and Shou, Y. (2017), "The modeling of crack propagation and coalescence in rocks under uniaxial compression using the novel conjugated bond-based peridynamics", *Int. J. Mech. Sci.*, **128**, 614-643.
Wang, Y., Zhou, X.P. and Xu, X. (2016), "Numerical simulation of propagation and coalescence of flaws in rock materials under compressive loads using the extended non-ordinary state-based peridynamics", *Eng. Fract. Mech.*, **163**, 248-273.
Wang, Y., Zhou, X., Wang, Y. and Shou, Y. (2018), "A 3-D conjugated bond-pair-based peridynamic formulation for initiation and propagation of cracks in brittle solids", *Int. J. Sol. Struct.*, **134**, 89-115.
Wang, Y., Zhou, X.P. and Kou, M. (2018), "Peridynamic investigation on thermal fracturing behavior of ceramic nuclear fuel pellets under power cycles", *Ceram. Int.*, **44**(10), 11512-11542.
Wang, X., Zhu, Z., Wang, M., Ying, P., Zhou, L. and Dong, Y. (2017), "Study of rock dynamic fracture toughness by using VB-SCSC specimens under medium-low speed impacts", *Eng. Fract. Mech.*, **181**, 52-64.
Wei, M.D., Dai, F., Xu, N.W., Xu, Y. and Xia, K. (2015), "Three-dimensional numerical evaluation of the progressive fracture mechanism of cracked chevron notched semi-circular bend rock specimens", *Eng. Fract. Mech.*, **134**, 286-303.
Whittaker, B., Singh, R. and Sun, G. (1992), *Rock Fracture Mechanics-Principles, Design and Applications*, Elsevier Science Publishers, Amsterdam, the Netherlands.
Yaylac, M. (2016), "The investigation crack problem through numerical analysis", *Struct. Eng. Mech.*, **57**(6), 1143-1156.
Yunteng, W., Zhou, X.P. and Shou, Y. (2017), "The modeling of crack propagation and coalescence in rocks under uniaxial compression using the novel conjugated bond-based peridynamics", *Int. J. Mech. Sci.*, **128**, 614-643.
Zare Naghadehi, M., Jimenez, R., Khalo Kakaie, R. and Jalali, S.M.E. (2011), "A probabilistic systems methodology to analyze the importance of factors affecting the stability of rock slopes", *Eng. Geol.*, **118**(3-4), 82-92.
Zhang, P. (2015), "Crack coalescence between two non-parallel flaws in rock-like material under uniaxial compression", *Eng. Geol.*, **199**, 74-90,
Zhao, C. (2015), "Analytical solutions for crack initiation on floor-strata interface during mining", *Geomech. Eng.*, **8**(2), 237-255.
Zhou, X.P., Bi, J. and Qian, Q.H. (2015), "Numerical simulation of crack growth and coalescence in rock-like materials containing multiple pre-existing flaws", *Rock Mech. Rock Eng.*, **48**(3), 1097-1114.
Zhou, X.P., Gu, X.B. and Wang, Y.T. (2015), "Numerical simulations of propagation, bifurcation and coalescence of cracks in rocks", *Int. J. Rock Mech. Min. Sci.*, **80**, 241-254.
Zhou, X.P. and Yang, H.Q. (2012), "Multiscale numerical modeling of propagation and coalescence of multiple cracks in rock masses", *Int. J. Rock Mech. Min. Sci.*, **55**, 15-27.

CC